Quantum critical behavior of the superfluid-Mott glass transition

Thomas Vojta, Jack Crewse, Martin Puschmann, Daniel Arovas, and Yury Kiselev

Quantum critical behavior of the superfluid-Mott glass transition

Thomas Vojta,[1] Jack Crewse,[1] Martin Puschmann,[1, 2] Daniel Arovas,[3] and Yury Kiselev[3]

[1]*Department of Physics, Missouri University of Science and Technology, Rolla, Missouri 65409, USA*
[2]*Institute of Physics, Technische Universität Chemnitz, 09107 Chemnitz, Germany*
[3]*Department of Physics, University of California, San Diego, La Jolla, California 92093, USA*
(Dated: September 12, 2016)

We investigate the zero-temperature superfluid to insulator transitions in a diluted two-dimensional quantum rotor model with particle-hole symmetry. We map the Hamiltonian onto a classical $(2+1)$-dimensional XY model with columnar disorder which we analyze by means of large-scale Monte Carlo simulations. For dilutions below the lattice percolation threshold, the system undergoes a generic superfluid-Mott glass transition. In contrast to other quantum phase transitions in disordered systems, its critical behavior is of conventional power-law type with universal (dilution-independent) critical exponents $z = 1.52(3)$, $\nu = 1.16(5)$, $\beta/\nu = 0.48(2)$, $\gamma/\nu = 2.52(4)$, and $\eta = -0.52(4)$. These values agree with and improve upon earlier Monte-Carlo results [Phys. Rev. Lett. 92, 015703 (2004)] while (partially) excluding other findings in the literature. As a further test of universality, we also consider a soft-spin version of the classical Hamiltonian. In addition, we study the percolation quantum phase transition across the lattice percolation threshold; its critical behavior is governed by the lattice percolation exponents in agreement with recent theoretical predictions. We relate our results to a general classification of phase transitions in disordered systems, and we briefly discuss experiments.

PACS numbers: 05.30.Jp, 64.60.Cn, 74.81.-g, 67.85.Hj

I. INTRODUCTION

Zero-temperature phase transitions between superfluid and insulating ground states in systems of disordered interacting bosons are prototypical quantum phase transitions with experimental applications ranging from helium absorbed in vycor[1,2] to Josephson junction arrays[3,4], superconducting films[5,6], doped quantum magnets in high fields[7–9], and to ultracold atoms in disordered optical lattices[10–12].

For generic disorder, the two bulk phases, viz. superfluid and Mott insulator, are separated by another phase, the Bose glass which is a compressible gapless insulator[13–15]. It can be understood as the Griffiths phase[16–18] of the superfluid-insulator transition in which rare large regions of local superfluid order coexist with the insulating bulk. The quantum phase transition between superfluid and Bose glass has been studied in great detail using various analytical and computational techniques. It has recently reattracted considerable attention because new analytical[19] and numerical[20–23] findings have challenged the scaling relation[13,14] $z = d$ between the dynamical exponent z and the space dimensionality d (Refs. 19–23 also contain long lists of references to earlier work.)

In the presence of particle-hole symmetry, the glassy Griffiths phase between superfluid and Mott insulator has a different character: it is the incompressible gapless Mott glass (also called the random-rod glass)[24,25]. The quantum phase transition between superfluid and Mott glass has attracted less attention than the Bose glass transition. Moreover, the available quantitative results for two space dimensions do not agree with each other. Monte Carlo simulations of a link-current model[26]

yielded a dynamical critical exponent $z = 1.5(2)$ and a correlation function exponent $\eta = -0.3(1)$.[27] A numerical strong-disorder renormalization group study of a particle-hole symmetric quantum rotor model gave $z = 1.31(7)$, a correlation length exponent $\nu = 1.09(4)$, and $\gamma/\nu = 1.1(2)$ where γ is the order parameter susceptibility exponent[28]. The Fisher relation $2 - \eta = \gamma/\nu$ then implies $\eta = 0.9(2)$. Furthermore, a recent Monte Carlo study of a quantum rotor model[29] reported good scaling by setting z to its clean value $z = 1$ which resulted in $\nu = 0.96(6)$. All these models are expected to be in the same universality class. The critical behavior of the superfluid-Mott glass quantum phase transition in two dimensions must thus be considered an open question.

To address this question, we consider a site-diluted two-dimensional quantum rotor model with particle-hole symmetry. After mapping this Hamiltonian onto a classical $(2+1)$-dimensional XY model with columnar defects, we perform large-scale Monte Carlo simulations for lattices with up to 11 million sites, averaging over 10 000 to 50 000 disorder configurations. The data are analyzed by a finite-size scaling technique[30–32] that does not require prior knowledge of the dynamical exponent z. We also include the leading corrections to scaling. Our results can be summarized as follows: The system features two distinct quantum phase transitions. For dilutions p below the percolation threshold p_c of the lattice, we find a superfluid-Mott glass transition characterized by universal (dilution-independent) critical behavior with exponent values $z = 1.52(3)$, $\nu = 1.16(5)$, $\beta/\nu = 0.48(2)$, $\gamma/\nu = 2.52(4)$, and $\eta = -0.52(4)$. The transition across the lattice percolation threshold p_c falls into a different universality class. Its simulation data can be fitted well with the theory developed in Ref. 33 which yields critical

exponents that can be expressed in terms of the classical percolation exponents and take the rational values $z = 91/48$, $\beta/\nu = 5/48$, $\gamma/\nu = 59/16$, and $\eta = -27/16$.

The rest of the paper is organized as follows. Section II introduces the quantum rotor Hamiltonian, the mapping to the classical XY model, and the finite-size scaling technique. Monte Carlo simulations for both the generic ($p < p_c$) transition and the percolation transition are discussed in Sec. III. We conclude in Sec. IV.

II. THEORY

A. Diluted rotor model

The starting point is a site-diluted quantum rotor model on a square lattice given by the Hamiltonian

$$H = \frac{U}{2} \sum_i \epsilon_i (\hat{n}_i - \bar{n}_i)^2 - J \sum_{\langle ij \rangle} \epsilon_i \epsilon_j \cos(\hat{\phi}_i - \hat{\phi}_j) . \quad (1)$$

Here, $\hat{n}_i$ is the number operator at site i, $\hat{\phi}_i$ is the phase operator, and U and J represent the charging energy and the Josephson coupling, respectively. $\bar{n}_i$ is the offset charge at site i. In the Josephson term, $\langle ij \rangle$ refers to pairs of nearest neighbors. The quenched random variables ϵ_i implement the site dilution. They are independent of each other and take the values 0 (vacancy) with probability p and 1 (occupied site) with probability $1 - p$.

As we are interested in the superfluid-Mott glass transition, we set all offset charges $\bar{n}_i$ to zero and consider commensurate (integer) filling $\langle \hat{n} \rangle$. In this case, the disorder is purely off-diagonal, and the model is particle-hole symmetric. The qualitative features of its phase diagram are well understood[14,25]. If the charging energy dominates, $U \gg J$, the ground state is a Mott insulator. In the opposite limit, $J \gg U$, the ground state is a superfluid as long as the dilution p is below the lattice percolation threshold p_c. For $p > p_c$, the lattice consists of disconnected clusters and a long-range ordered superfluid state is impossible.

In the case of particle-hole symmetry, the quantum rotor model (1) can be mapped[34] onto a classical $(2 + 1)$-dimensional XY model on a cubic lattice having the Hamiltonian

$$H_{cl} = -J_s \sum_{\langle i,j \rangle, t} \epsilon_i \epsilon_j \mathbf{S}_{i,t} \cdot \mathbf{S}_{j,t} - J_\tau \sum_{i,t} \epsilon_i \mathbf{S}_{i,t} \cdot \mathbf{S}_{i,t+1} \quad (2)$$

where $\mathbf{S}_{i,t}$ is an O(2) unit vector at the lattice site with spatial coordinate i and "imaginary time" coordinate t. The coupling constants J_s/T and J_τ/T are determined by the original quantum rotor Hamiltonian (1) with T being an effective "classical" temperature, not equal to the real physical temperature. (The physical temperature of the quantum system (1) maps onto the inverse system size in imaginary time direction of the classical model.) Due to universality, the exact values of J_s and J_τ are
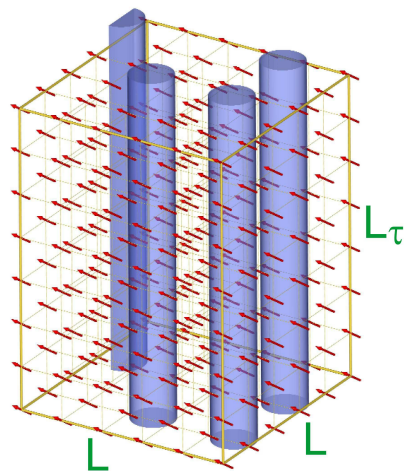

FIG. 1. Sketch of the classical XY model (2). The arrows represent the classical unit vectors $\mathbf{S}$, and the tubes show the locations of the vacancy columns.

not important for the critical behavior. We therefore set $J_s = J_\tau = 1$ and drive the XY model (2) through the transition by varying the classical temperature T. Because the vacancy positions do not depend on the imaginary time coordinate t, the defects in the classical model (2) are columnar, i.e., the disorder is perfectly correlated in the imaginary time direction (see Fig. 1).

In the clean undiluted limit $p = 0$, the Hamiltonian (2) simplifies to the usual three-dimensional XY model. The correlation length critical exponent of the three-dimensional XY universality class takes the value $\nu \approx 0.6717$ (see, e.g., Ref. 35). This value violates the Harris criterion[36] $d\nu > 2$ where $d = 2$ is the number of dimensions in which there is randomness. Consequently, the three-dimensional clean XY critical point is unstable against columnar defects, and we expect the diluted system to feature a different critical behavior.

B. Anisotropic finite-size scaling

Finite-size scaling[37,38] is a powerful tool for analyzing Monte Carlo data. Particularly useful are quantities of scale dimension zero such as the (average) Binder cumulant

$$g_{av} = \left[1 - \frac{\langle |\mathbf{m}|^4 \rangle}{3 \langle |\mathbf{m}|^2 \rangle^2} \right]_{dis} , \quad (3)$$

where $\mathbf{m} = (1/N) \sum_{i,\tau} \mathbf{S}_{i,\tau}$ is the order parameter (N denotes the number of lattice sites). $[\ldots]_{dis}$ refers to the disorder average and $\langle \ldots \rangle$ denotes the Monte Carlo average for each sample. In an isotropic system with a single relevant length scale, it takes the scaling form $g_{av}(r, L) = X(rL^{1/\nu})$. Here L is the linear system size, $r = (T - T_c)/T_c$ is the distance from criticality, and X is a scaling function. This scaling form implies that g_{av} vs.

r curves for systems of different sizes L all cross at criticality, $r = 0$, having the value $g_{av}(0, L) = X(0)$. This can be used to find the critical point with high accuracy. Moreover, the slopes of the g_{av} vs. r curves at $r = 0$ vary as $L^{1/\nu}$ which can be used to measure ν.

As the quenched disorder in our Hamiltonian (2) breaks the symmetry between the space and imaginary time directions, we need to distinguish the linear system size L in the two space directions from the size L_τ in the imaginary time direction. (L_τ corresponds to the inverse physical temperature of the original quantum model (1).) If the putative disordered critical point fulfills conventional power-law dynamical scaling, the finite-size scaling form of the average Binder cumulant then reads

$$g_{av}(r, L, L_\tau) = X_{g_{av}}(rL^{1/\nu}, L_\tau/L^z) \qquad (4)$$

where z is the dynamical critical exponent, and $X_{g_{av}}$ is the dimensionless scaling function which now depends on two arguments. Note that some quantum phase transitions in disordered systems feature exotic activated dynamical scaling instead of power-law scaling, for example the ferromagnetic transition in the random transverse-field Ising model[39], the pairbreaking superconductor-metal quantum phase transition[40–42], and magnetic transitions in itinerant systems[43,44]. For activated dynamical scaling, the scaling combination L_τ/L^z in Eq. (4) needs to be replaced by $\ln(L_\tau)/L^\psi$ where ψ is the tunneling exponent. Based on the classification of disordered quantum phase transitions developed in Refs. 18 and 45, we do not expect the superfluid-Mott glass transition to show activated scaling. We will return to this point in the concluding section.

How can one perform a finite-size scaling analysis of Monte Carlo data based on the scaling form (4) of the average Binder cumulant? If the value of z is known, the analysis is as simple as in the isotropic case: One chooses system sizes L and L_τ such that $L_\tau = c\, L^z$ were c is a constant. Then the g_{av} vs. r curves for systems of different sizes cross at criticality [with the value $g_{av}(0, L, c\, L^z) = X_{g_{av}}(0, c)$] which can be used to locate the critical point. However, in the absence of a value for z, this approach breaks down because the correct shapes (aspect ratios) of the samples are not known.

A method for finding the correct sample shape within the simulations[30–32] can be based on the following property of the Binder cumulant: For fixed L, g_{av} as a function of L_τ has a peak at position L_τ^{max} and value g_{av}^{max}. The peak position marks the *optimal* sample shape, where the ratio L_τ/L behaves like the corresponding ratio of the correlation lengths in time and space directions, ξ_τ/ξ_s. (If the aspect ratio deviates from the optimal one, the system can be decomposed into independent units either in space or in time direction, and thus g_{av} decreases.) At criticality, L_τ^{max} must be proportional to L^z, fixing the second argument of the scaling function $X_{g_{av}}$. This implies that the peak value g_{av}^{max} at criticality is independent of L and that the g_{av} vs. r curves of samples of the optimal shape ($L_\tau = L_\tau^{max}$) cross at $r = 0$.

In our simulations, we use an iterative approach. We start from a guess for z and the corresponding sample shapes. The approximate crossing of the g_{av} vs. r curves for these samples gives an estimate for T_c. At this temperature, we next analyze g_{av} as a function of L_τ for fixed L. The values of L_τ^{max} give improved estimates for the optimal sample shapes and thus for z. After iterating this procedure three or four times, the values of T_c and z will have converged with reasonable accuracy.

Once z and T_c are determined, the finite-size scaling analysis proceeds as usual, based on the scaling forms

$$m = L^{-\beta/\nu} X_m(rL^{1/\nu}, L_\tau/L^z) , \qquad (5)$$

$$\chi = L^{\gamma/\nu} X_\chi(rL^{1/\nu}, L_\tau/L^z) \qquad (6)$$

for the order parameter m and its susceptibility χ. Here, X_m and X_χ are dimensionless scaling functions, and β and γ are the order parameter and susceptibility critical exponents, respectively.

In addition to these thermodynamic quantities, we also calculate the correlation lengths ξ_s and ξ_τ is the space and imaginary time directions, respectively. They are obtained, as usual, from the second moment of the spin-spin correlation function[46–48] and can be expressed in terms of the Fourier transform $\tilde{G}(q_s, q_\tau)$ of the correlation function,

$$\xi_s = \left[\left(\frac{\tilde{G}(0,0) - \tilde{G}(q_{s0}, 0)}{q_{s0}^2 \tilde{G}(q_{s0}, 0)} \right)^{1/2} \right]_{dis} , \qquad (7)$$

$$\xi_\tau = \left[\left(\frac{\tilde{G}(0,0) - \tilde{G}(0, q_{\tau0})}{q_{\tau0}^2 \tilde{G}(0, q_{\tau0})} \right)^{1/2} \right]_{dis} . \qquad (8)$$

Here, $q_{s0} = 2\pi/L$ and $q_{\tau0} = 2\pi/L_\tau$ are the minimum values of the wave numbers q_s and q_τ that fit into a system of linear size L and L_τ in space and imaginary time direction, respectively. The reduced correlation lengths ξ_s/L and ξ_τ/L_τ have scale dimension zero, their scaling forms therefore read

$$\xi_s/L = X_{\xi_s}(rL^{1/\nu}, L_\tau/L^z) , \qquad (9)$$

$$\xi_\tau/L_\tau = X_{\xi_\tau}(rL^{1/\nu}, L_\tau/L^z) . \qquad (10)$$

III. MONTE CARLO SIMULATIONS

A. Overview

Our Monte Carlo simulations of the classical XY model (2) combine the Wolff cluster algorithm[49] with conventional Metropolis updates[50]. Specifically, a full Monte Carlo sweep consists of a Metropolis sweep over the lattice followed by a Wolff sweep. (A Wolff sweep is defined as a number of cluster flips such that the total number of flipped spins equals the number of lattice sites.) The Wolff algorithm greatly reduces the critical slowing down, and the Metropolis updates equilibrate small
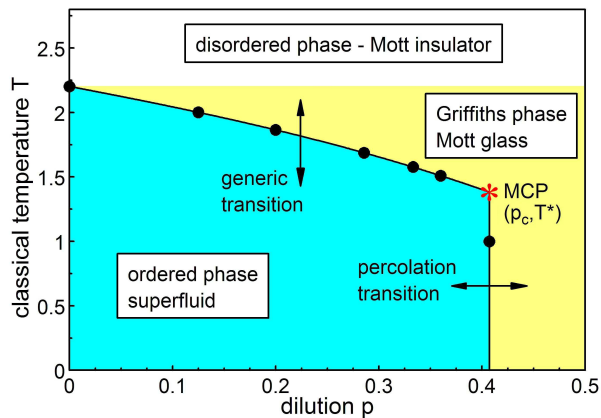
FIG. 2. (Color online) Phase diagram of the classical XY model (2) as a function of classical temperature and dilution. MCP is the multicritical point that separates the generic and percolation transitions. The big dots mark the numerically determined transition points. The lines are guides for the eye only.

disconnected clusters of sites that are missed in the construction of the Wolff clusters (this becomes important at higher dilutions p).

We simulate systems with linear sizes up to $L = 150$ in space direction and up to $L_\tau = 1792$ in the imaginary time direction at dilutions $p = 0$, $1/8$, $1/5$, $2/7$, $1/3$, $9/25$ and the percolation threshold $p_c = 0.407253$.

The simulation of disordered systems requires a high numerical effort because many samples with different disorder configurations need to be studied to compute averages, variances, and distributions of observables. For good performance, one must thus carefully optimize the number n_s of samples (i.e., disorder configurations) and the number n_m of measurements during the simulation of each sample. Based on the consideration in Refs. 32, 51–53, we have chosen rather short runs of $n_m = 500$ full sweeps per sample (with a measurement after each sweep) but large numbers of disorder configurations ranging from $n_s = 10\,000$ to $50\,000$ depending on the system size. The equilibration period is taken to be 100 full sweeps, significantly longer than the actual equilibration times that reach 30 to 40 sweeps at maximum. Short Monte Carlo runs can lead to biases in some of the observables. To eliminate these, we have implemented improved estimators along the lines discussed in the appendix of Ref. 53.

The phase diagram resulting from these simulations is shown in Fig. 2. The critical temperature $T_c(p)$ decreases with increasing dilution from its clean value $T_c(0)$, as expected. For dilutions above the percolation threshold $p_c = 0.407253$, the lattice consists of disconnected finite-size clusters. Therefore, long-range superfluid order is impossible. Right at p_c, there is an infinite cluster of dimension $1 + d_f$ where $d_f = 91/48$ is the dimensionality of the critical percolation cluster in two dimensions, and

the extra 1 stems from the imaginary time direction. As $1 + d_f$ is larger than the lower critical dimension $d_c^- = 2$ of the XY model, the XY model on the critical percolation cluster orders below a multicritical temperature T^*. This implies that the phase boundary coincides with the classical percolation threshold for $T < T^*$ (see also Ref. 54). We thus identify two different phase transitions, (i) the generic superfluid-Mott glass transition for $p < p_c$ and (ii) a percolation transition across the lattice percolation threshold.

In the following sections, we discuss the critical behaviors of these transitions in detail. To test our codes, we have also studied the clean limit $p = 0$ using system sizes up to 224^3 sites. By analyzing the crossings of the Binder cumulant and the reduced correlation length, we find a critical temperature $T_c(0) = 2.201844(4)$. Finite-size scaling then gives the critical exponents $\beta/\nu = 0.518(3)$, $\gamma/\nu = 1.961(3)$, and $\nu = 0.673(2)$. Within their errors, they agree well with high-precision results for the three-dimensional XY universality class[35].

As a further test for the universality of the (generic) critical behavior, we also perform exploratory simulations of a soft-spin version of the classical Hamiltonian. They are discussed in Sec. III D.

B. Generic superfluid-Mott glass transition

To analyze the critical behavior of the generic transition occurring for $0 < p < p_c$, we consider five different dilutions, $p = 1/8$, $1/5$, $2/7$, $1/3$, and $9/25$. As described in Sec. II B, we use an iterative procedure that consists of two types of simulation runs. The first are runs right at T_c for systems with several different L_τ for each L. Finite-size scaling of the Binder cumulant at T_c as a function of L and L_τ gives the optimal sample shapes and the dynamical exponent z. In the second set of simulations, we vary the temperature over a range in the vicinity of T_c, but we consider only the optimal shapes found in the first part. Finite-size scaling of the order parameter, susceptibility, Binder cumulant, and correlation length as functions of L and T then yields the critical exponents β/ν, γ/ν, and ν.

The inset of Fig. 3 shows the Binder cumulant g_{av} as a function of L_τ for several $L = 10$ to 100 at the estimated critical temperature $T_c = 1.577$ for dilution $p = 1/3$. As expected at the critical point, the maximum Binder cumulant g_{av}^{max} for each of the curves does not depend on L. (The remaining weak variation visible in the figure can be attributed to corrections to scaling, see below.) To generate a scaling plot that tests the scaling form (4), we now fit each g_{av} vs. L_τ curve with an inverted parabola in $\ln L_\tau$. The vertex of this parabola yields the position L_τ^{max} of the maximum and its value g_{av}^{max}. When plotting g_{av}/g_{av}^{max} vs. L_τ/L_τ^{max} the data scale very well, as can be seen in the resulting scaling plot in the main panel of Fig. 3. This demonstrates that the Binder cumulant fulfills Eq. (4) with high accuracy. We have
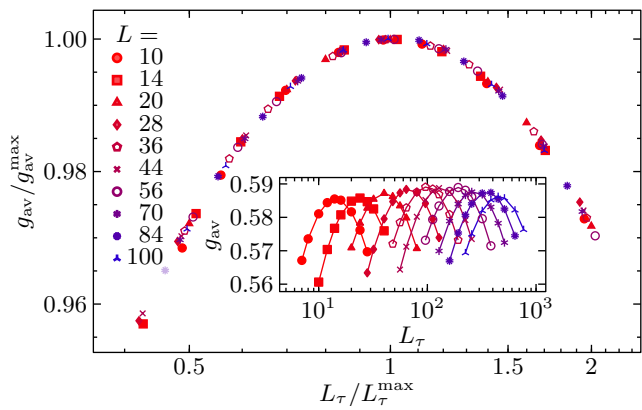
FIG. 3. (Color online) Binder cumulant g_{av} as a function of L_τ for several L at the critical temperature $T_c = 1.577$ for dilution $p = 1/3$. The relative statistical error of g_{av} is between 0.05% and 0.1%. Inset: Raw data g_{av} vs. L_τ. Main panel: Scaling plot g_{av}/g_{av}^{max} vs. L_τ/L_τ^{max}.
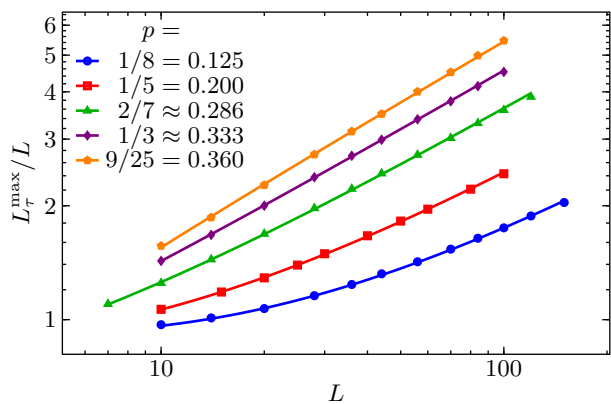

FIG. 4. (Color online) Double logarithmic plot of L_τ^{max}/L vs. L for several dilutions p below the percolation threshold. Solid lines at fits to $L_\tau^{max} = aL^z(1+bL^{-\omega})$ giving $z = 1.526(5)$ and $\omega = 0.76(2)$. The statistical errors of the data are well below a symbol size (The statistical error of L_τ^{max} is determined by repeating the scaling analysis for 1000 synthetic data sets that add to the original data set a Gaussian random noise that corresponds to the uncertainties of the data.)

created the corresponding scaling plots for all the other dilutions, $p = 1/8$, $1/5$, $2/7$, and $9/25$, with analogous results.[55]

To determine the dynamical critical exponent z, we now analyze the dependence of the positions L_τ^{max} of the maximum on L. According to Eq. (4), we expect the power-law dependence $L_\tau^{max} \sim L^z$. In Fig. 4, we plot L_τ^{max} vs. L for all dilutions $p < p_c$. The curves show significant deviations from pure power-law behavior, in particular for the smaller dilutions, indicating that the crossover from clean to disordered critical behavior is slow. The resulting corrections to scaling are strong and cannot be neglected. Pure power-law fits of the data would therefore only yield effective, scale-

dependent exponents. To determine the true asymptotic exponents, we include the leading corrections to scaling via the ansatz $L_\tau^{max} = aL^z(1 + bL^{-\omega})$ with universal (dilution-independent) critical exponents z and ω but dilution-dependent prefactors a and b. The exponent values resulting from a combined fit of the data for all five dilutions are $z = 1.526(5)$ and $\omega = 0.76(2)$. The fit is of good quality giving $\tilde\chi^2 \approx 1.4$. [We denote the reduced sum of squared errors of the fit (per degree of freedom) by $\tilde\chi^2$ to distinguish it from the susceptibility χ.] The fit is also robust against removing complete data sets or removing points from the upper or lower end of each set. Interestingly, the leading corrections to scaling appear to vanish somewhere between $p = 1/3$ and $9/25$, as the prefactor b of the correction term changes sign. Correspondingly, pure power-law fits of the $p = 1/3$ and $9/25$ data yield $z = 1.502$ and 1.546, respectively. These values are close to the estimate from the combined fit and nicely bracket it on both sides. An additional significant source of errors is the uncertainty of the critical temperature. To assess its effect on the dynamical exponent, we repeat the L_τ^{max} vs. L analysis (for dilutions $p = 1/3$ and $9/25$) at temperatures slightly above and below our estimated T_c ($\Delta T_c \approx 0.003$, roughly at the boundaries of our confidence intervals). This leads to shifts in z of about 0.01 to 0.02. Our final estimate for the dynamical critical exponent therefore reads $z = 1.52(3)$.

To find the remaining critical exponents, we now turn to the Monte Carlo runs that use the optimal sample shapes (L, L_τ^{max}). According to Eqs. (5) and (6), β/ν and γ/ν can be obtained from the L dependence of the order parameter and susceptibility at T_c of the optimally shaped samples. As we expect corrections to scaling to be important, we again include subleading terms in our fit functions, $m = aL^{-\beta/\nu}(1+bL^{-\omega})$ for the order parameter and $\chi = aL^{\gamma/\nu}(1+bL^{-\omega})$ for the susceptibility. Here β/ν, γ/ν, and ω are the universal, dilution-independent critical exponents while the coefficients a and b are again non-universal. (Note that a and b generally differ from quantity to quantity; we use the same symbols to avoid cluttering up the notation too much.) When performing fits of our data to these expressions, we noticed, however, that the quality of the fits is extremely sensitive to small changes of the estimates for T_c (much more so than in the analysis of the dynamical exponent z above). To determine higher accuracy estimates of T_c, we use the criterion that the value of g_{av}^{max} at criticality should approach a *dilution-independent* constant with $L \to \infty$ at a universal critical point. Varying T until this criterion is fulfilled yields improved estimates for the critical temperatures, viz. $T_c = 1.9989$ for $p = 1/8$, $T_c = 1.8603$ for $p = 1/5$, $T_c = 1.6838$ for $p = 2/7$, $T_c = 1.5735$ for $p = 1/3$, and $T_c = 1.5049$ for $p = 9/25$. We estimate the error of these values to be about 0.001. Figure 5 shows the resulting dependence g_{av}^{max} on L. In the large-L limit, g_{av}^{max} approaches the value 0.599(2). Note that the non-monotonic behavior of g_{av}^{max} for weak dilutions suggests that at least two corrections to scaling terms contribute

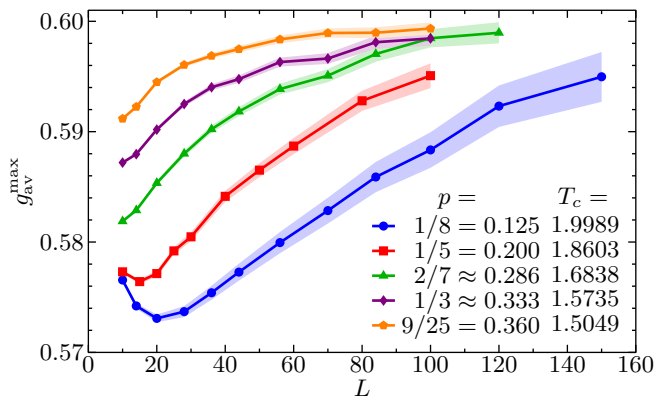FIG. 5. (Color online) g_{av}^{max} vs. L at the improved estimates for T_c. The statistical errors of the data points are about a symbol size or smaller. The shading represents the range of g_{av}^{max} values for temperatures T within $T_c \pm 0.0002$ and is intended to illustrate to what extent the extrapolation depends on T. Based on these data we estimate that the error of T_c does not exceed 0.001.

FIG. 7. (Color online) Double logarithmic plot of χ vs. L for several dilutions p below the percolation threshold. Solid lines at fits to $\chi = aL^{\gamma/\nu}(1+bL^{-\omega})$ giving $\gamma/\nu = 2.524(8)$ and $\omega = 0.77(1)$. The lines are dotted in the regions not included in the fit. The statistical errors of the data are well below a symbol size.
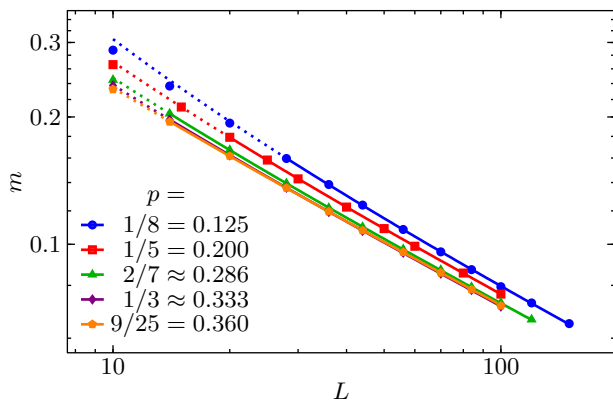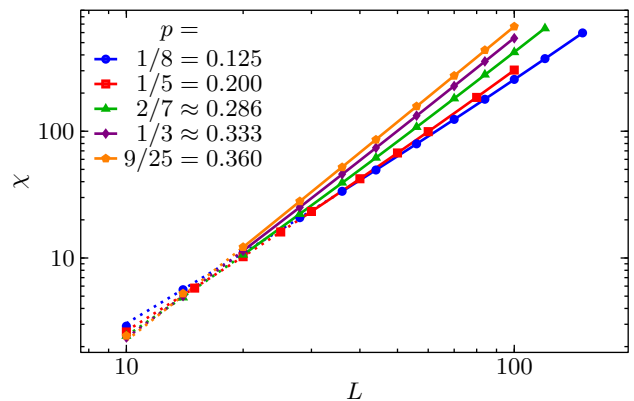

FIG. 6. (Color online) Double logarithmic plot of m vs. L for several dilutions p below the percolation threshold. Solid lines at fits to $m = aL^{-\beta/\nu}(1 + bL^{-\omega})$ giving $\beta/\nu = 0.480(8)$ and $\omega = 0.82(2)$. The lines are dotted in the regions not included in the fit. The statistical errors of the data are well below a symbol size.
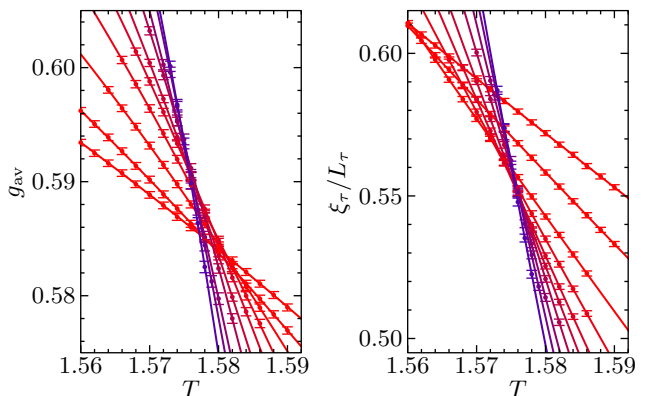

FIG. 8. (Color online) Average Binder cumulant g_{av} and reduced correlation length ξ_τ/L_τ as functions of temperature for dilution $p = 1/3$ and systems of optimal shape. System sizes range from $L = 10$ to 100 (as listed in Fig. 3) with increasing slope.

at small L.

Using the improved critical temperatures, we now proceed to determine β/ν and γ/ν. Figure 6 shows the order parameter m at T_c as a function of L for all dilutions $p < p_c$. The combined fit of all data to $m = aL^{-\beta/\nu}(1+bL^{-\omega})$ is of good quality ($\tilde{\chi}^2 \approx 0.64$) if the smallest system sizes are excluded (see figure). Interestingly, the sizes that need to be excluded are exactly those for which g_{av}^{max} in Fig. 5 appears to be dominated by the second subleading correction to scaling term.) The exponents resulting from the fit read $\beta/\nu = 0.480(8)$ and $\omega = 0.82(2)$. To assess the error arising from the uncertainty in T_c, we repeat the analysis for temperatures $T_c \pm \Delta T_c$ with $\Delta T_c = 0.001$. This leads to shifts of β/ν of about 0.01. Our final estimate therefore reads $\beta/\nu = 0.48(2)$.

The system-size dependence of the order parameter susceptibility χ at criticality is presented in Fig. 7 for all dilutions $p < p_c$. After excluding the smallest system sizes (see figure), the combined fit of all data to $\chi = aL^{\gamma/\nu}(1 + bL^{-\omega})$ is again of good quality ($\tilde{\chi}^2 \approx 1.5$) and yields the exponents $\gamma/\nu = 2.524(8)$ and $\omega = 0.77(1)$. After including potential errors from the uncertainty in T_c and the fit range, the final exponent estimate is $\gamma/\nu = 2.52(4)$.

So far, the analysis has focused on the behavior right at T_c. To find a complete set of critical exponents, we now determine the correlation length exponent ν which requires off-critical data. Figure 8 shows the temperature dependence of the Binder cumulant g_{av} and the reduced correlation length ξ_τ/L_τ for systems of optimal shape but different sizes at dilution $p = 1/3$. Both quantities
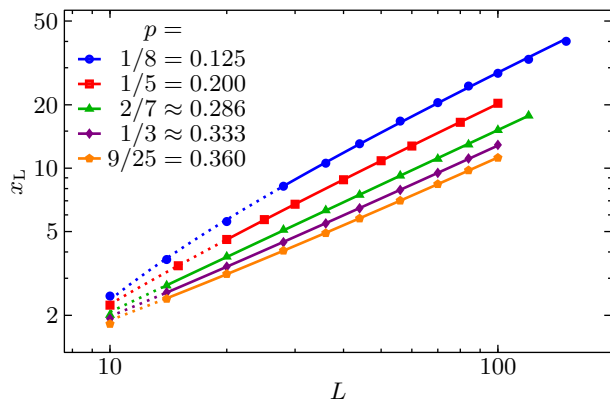
FIG. 9. (Color online) Slope $x_L = (d/dT)\xi_\tau/L_\tau$ at criticality vs. system size L for optimally shaped samples at different dilutions p. Solid lines at fits to $x_L = aL^{1/\nu}(1+bL^{-\omega})$ giving $\nu = 1.165(6)$ and $\omega = 0.74(1)$. The lines are dotted in the regions not included in the fit.
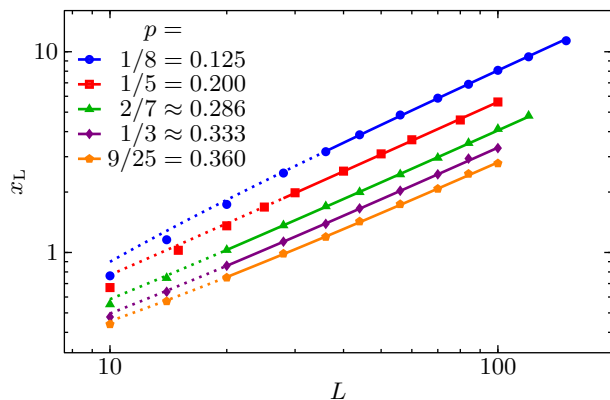

FIG. 10. (Color online) Slope $x_L = (d/dT)g_{av}$ at criticality vs. system size L for optimally shaped samples at different dilutions p. Solid lines at fits to $x_L = aL^{1/\nu}(1+bL^{-\omega})$ giving $\nu = 1.146(16)$ and $\omega = 0.97(23)$. The lines are dotted in the regions not included in the fit.

have scale dimension zero, therefore, the curves for different system sizes are expected to cross at the critical temperature T_c. The figure demonstrates that the crossings for both quantities shift with increasing L, reflecting significant corrections to scaling. According to Eqs. (4) and (8), the slopes $(d/dT)g_{av}$ and $(d/dT)\xi_\tau/L_\tau$ at the critical temperature T_c vary as $L^{1/\nu}$ with system size. To extract the slopes, we fit straight lines (for ξ_τ/L_τ) or quadratic parabolas (for g_{av}) to the data close to T_c. The resulting slopes are shown as a function of system size in Figs. 9 and 10, respectively. The exponent ν is now obtained from fits of the slopes to the form $aL^{-1/\nu}(1 + bL^{-\omega})$. In the case of the reduced correlation length ξ_τ/L_τ (Fig. 9) a combined fit of all dilutions $p < p_c$ is of good quality after the smallest system sizes have been excluded ($\tilde{\chi}^2 \approx 1.2$) and yields $\nu = 1.165(6)$ as well as $\omega = 0.74(1)$. The corresponding fit of the slopes

of the Binder cumulant has a somewhat poorer quality ($\tilde{\chi}^2 \approx 5.5$) and is not very stable with respect to adding and removing data points at the ends of the interval. The resulting exponents $\nu = 1.146(16)$ and $\omega = 0.97(23)$ have therefore larger errors. In addition to the slopes of the Binder cumulant g_{av} and the reduced correlation length ξ_τ/L_τ at T_c, we have also studied the slopes of ξ_s/L and $\ln m$ (not shown). After we account for the differences between all these estimates and include potential errors from the uncertainty in T_c (by repeating the analysis at temperatures $T_c \pm 0.001$) we arrive at the final estimate $\nu = 1.16(5)$. This value fulfills the inequality[56] $d\nu > 2$.

The critical exponents β/ν, γ/ν, and z are not independent of each other as they must fulfill the hyperscaling relation $2\beta/\nu + \gamma/\nu = d + z$ where $d = 2$ is the space dimensionality. Our values, $\beta/\nu = 0.48(2)$, $\gamma/\nu = 2.52(4)$, and $z = 1.52(3)$ fulfill this relation within their error bars. We also note that all our estimates for the leading irrelevant exponent ω are roughly consistent with each other, giving us confidence that our results represent true asymptotic rather than effective critical exponents.

C. Percolation transition

We now turn to the percolation transition that occurs when the system is tuned through the percolation threshold p_c at low (classical) temperatures (see Fig. 2). The critical behavior of this transition stems from the critical geometry of the percolating lattice while the dynamical fluctuations of the rotor variables are uncritical and "just go along for the ride" (the rotor model on each of the percolation clusters is locally ordered). Vojta and Schmalian[33] developed a theory of this percolation quantum phase transition. It predicts critical behavior governed by the lattice percolation exponents. For two space dimensions it yields the exact exponent values $\beta = 5/36$, $\gamma = 59/12$, $\nu = 4/3$, and $z = 91/48$.

To test these predictions, we perform simulations at dilution $p = p_c = 0.407253$ and temperature $T = 1.0$. These calculations require a particularly high numerical effort, because the large value of z leads to a rapid increase with L of the optimal system size L_τ^{max} in imaginary time direction. We have thus restricted the simulations to sizes up to $L = 56$ and $L_\tau = 1792$ using between 10 000 and 50 000 disorder configurations.

The data analysis proceeds in analogy to Sec. III B. We obtain L_τ^{max} from the maxima of the Binder cumulant g_{av} as a function of L_τ at fixed L. In Fig. 11, we present a plot of L_τ^{max} vs. L. The data can be fitted with high quality ($\tilde{\chi}^2 \approx 0.4$) to the predicted power law $L_\tau^{max} \sim L^{91/48}$. After having found L_τ^{max}, we calculate the order parameter and susceptibility right at criticality for optimally shaped samples of different sizes. The resulting data are also presented in Fig. 11. The susceptibility data can be fitted well to the predicted power law $\chi \sim L^{59/16}$ giving $\tilde{\chi}^2 \approx 0.8$. The exponent $\beta/\nu = 5/48$ is very small, corresponding to a slow decay of the order
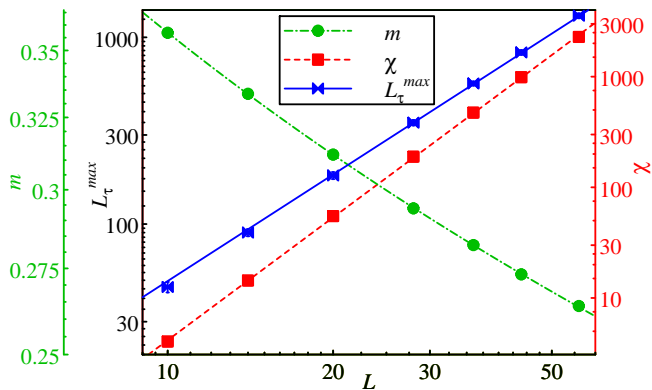
FIG. 11. (Color online) Double logarithmic plots of $L_\tau^{\max}$, m and χ for dilution $p = p_c = 0.407253$ and $T = 1.0$. The lines are fits to the predictions of the Ref. 33, namely $L_\tau^{\max} \sim L^{91/48}$ and $\chi \sim L^{59/16}$. For the order parameter, a subleading correction is included via $m = aL^{-5/48}(1 + bL^{-\omega})$. The statistical errors are of the order of the symbol size or smaller.
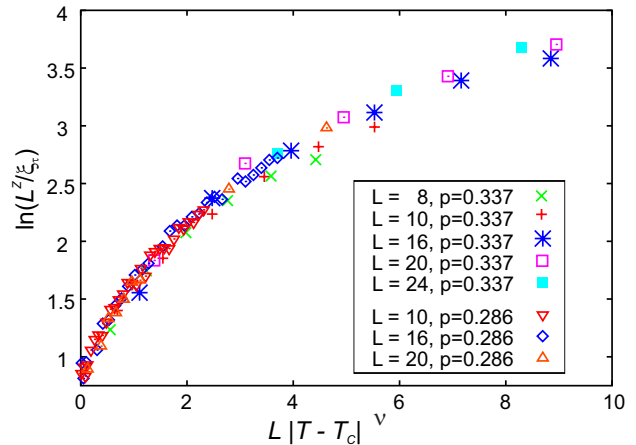

FIG. 12. (color online) Scaling plot of the correlation length ξ_τ in imaginary time direction of the soft-spin model (11). Shown are data for two dilutions p, several system sizes L, and temperatures T on the disordered side of the transition. The exponents z and ν are fixed at the values found in Sec. III B. The data are averages over 100 disorder configurations. Their statistical errors are about one symbol size.

parameter m with L. Subleading corrections are thus much more visible as indicated by the curvature of the m vs. L curve in Fig. 11. We have therefore fitted the order parameter to $m = aL^{-5/48}(1 + bL^{-\omega})$. This fit is again of high quality, with $\tilde{\chi}^2 \approx 0.5$.

Our simulation data thus agree nearly perfectly with the critical behavior predicted in Ref. 33.

D. Soft-spin model

We also consider a soft-spin version of the classical Hamiltonian to test whether or not its critical exponents agree with those of the hard-spin model analyzed above, as is expected from universality. The soft-spin Hamiltonian reads

$$H_{\text{soft}} = -\sum_{\langle i,j \rangle, t} \epsilon_i \epsilon_j \mathbf{S}_{i,t} \cdot \mathbf{S}_{j,t} - \sum_{i,t} \epsilon_i \mathbf{S}_{i,t} \cdot \mathbf{S}_{i,t+1}$$
$$- \frac{1}{2} \sum_{i,t} \epsilon_i |\mathbf{S}_{i,t}|^2 + \sum_{i,t} \epsilon_i \left(|\mathbf{S}_{i,t}|^2 \right)^2 \quad (11)$$

where $\mathbf{S}_{i,t}$ now represents an unrestricted two-component vector. We perform Monte-Carlo simulations of this soft-spin model using the efficient Worm algorithm[57], studying dilutions $p = 0.286$ and 0.337. The system sizes range from $L = 8$ to 24 with L_τ fixed at $L_\tau = L^z$ using the dynamical exponent value found in Sec. III B[58].

We now analyze the correlation length ξ_τ in imaginary time direction (equivalent to the inverse energy gap of the corresponding quantum model) on the disordered side of the phase transition. According to Eq. (10), its scaling form for samples of shape $L_\tau = L^z$ can be written as $\xi_\tau = L^z X_{\xi_\tau}(rL^{1/\nu}, 1)$. Thus, if we plot ξ_τ/L^z vs. $(T - T_c)L^{1/\nu}$, the data for different sizes and temperatures should all fall onto a single master curve. Figure

12 presents such a plot for two site dilutions p, with the critical exponents z and ν fixed at the values found in Sec. III B. Within their statistical errors, the data scale well. Consequently, even though we have not independently determined the critical exponents of the soft-spin model (11), the Monte Carlo data are compatible with the critical behavior found earlier.

IV. CONCLUSIONS

In summary, we have carried out large-scale computer simulations to determine the critical behavior of the superfluid-Mott glass quantum phase transition in two space dimensions. To this end, we have mapped a quantum rotor model with commensurate filling and off-diagonal disorder onto a (2+1)-dimensional classical XY model with columnar defects. We have then analyzed this classical system by means of Monte Carlo methods.

The corresponding clean superfluid-Mott insulator transition is in the three-dimensional XY universality class; its correlation length exponent $\nu \approx 0.6717$ violates the Harris criterion $d\nu > 2$ with $d = 2$. The clean critical behavior is therefore expected to be unstable against the columnar disorder. Accordingly, we have found that the critical behavior of the superfluid-Mott glass transition differs from that of the clean superfluid-Mott insulator transition.

In contrast to other quantum phase transitions in disordered systems[39–44], the superfluid-Mott glass transition features a conventional finite-disorder critical point whose dynamical scaling is characterized by a power-law relation $\xi_\tau \sim \xi_s^z$ between the correlation lengths in the space and time directions (rather than an infinite-

Value	This work	Ref. 26	Ref. 28	Ref. 29
ν	1.16(5)		1.09(4)	0.96(6)
z	1.52(3)	1.5(2)	1.31(7)	fixed at 1
β/ν	0.48(2)	*0.60(15)*	*1.1(2)*	
γ/ν	2.52(4)	*2.3(1)*	1.1(2)	
η	*−0.52(4)*	−0.3(1)	*0.9(2)*	

TABLE I. Critical exponents of the superfluid-Mott glass quantum phase transition. Upright numbers are directly given in the respective papers, italic ones were calculated using scaling relations such as $2\beta/\nu + \gamma/\nu = d + z$ and $\eta = 2 - \gamma/\nu$.

randomness critical point with activated dynamical scaling for which ξ_τ would grow exponentially with ξ_s). This result agrees with the general classification of phase transitions in disordered systems based on the rare region (or defect) dimensionality[18,45]. In terms of the mapped, classical Hamiltonian (2), the rare regions in our problem are one-dimensional rods with XY order-parameter symmetry. As the lower-critical dimension of the classical XY model is $d_c^- = 2$, the rare region dimensionality fulfills $d_{RR} < d_c^-$, putting the system into the conventional class A of the classification.

For the generic transition occurring at dilutions p below the lattice percolation threshold p_c, our Monte Carlo data are described well by a universal critical behavior with dilution-independent critical exponents. The numerical estimates of the exponent values are summarized in Table I and compared to earlier results in the literature. Our results are in reasonable agreement with (but more accurate than) Monte Carlo simulations of a link-current model[26] that is expected to be in the same universality class as our Hamiltonian. The results in Ref. 28 were obtained using a numerical implementation of the strong-disorder renormalization group. This method is expected to give approximate rather than exact results at a conventional finite-disorder critical point such as the one under consideration here. In view of this, the agreement of ν and z can be considered satisfactory. However, the values of β/ν, γ/ν, and η (that all involve the scale dimension of the order parameter) are far away from the Monte Carlo results in this work and in Ref. 26. Our findings are also incompatible with the clean value $z = 1$ that was assumed in Ref. 29.

It is interesting to consider the evolution of the dynamical exponent z with the order parameter dimensionality.

The deviation of z from the clean value, which is $z = 1$ for any number of components, can be understood as a measure of the strength of the disorder effects. In the (2+1)-dimensional Heisenberg model (three order parameter components) with columnar defects, the exponent takes the value[32] $z = 1.31$. The (2+1)-dimensional XY model (two components) studied in the present paper has $z = 1.52$, while the corresponding Ising model[59] (one component) features activated scaling that corresponds to $z = \infty$. The value of z thus increases monotonically with decreasing order parameter dimensionality.

In addition to the generic superfluid-Mott glass transition that occurs for dilutions $p < p_c$, we have also investigated the percolation quantum phase transition across p_c. Here, our Monte Carlo data agree very well with the predictions of the scaling theory by Vojta and Schmalian[33].

Potential routes to study the superfluid-Mott glass transition in experiment include disordered bosonic systems in ultracold atoms as well as dirty and granualar superconductors (for some superconductor-insulator transitions, there is experimental and numerical evidence for the bosonic nature of the transition). In these systems, it may be hard, though, to fulfill the condition of exact particle-hole symmetry in the presence of disorder. *Statistical* particle hole symmetry may be easier to achieve, but it is not fully resolved whether or not it would destabilize the Mott glass and turn it into a Bose glass[25,60,61].

Another type of experimental systems that contain Mott-glass physics are diluted anisotropic spin-1 antiferromagnets[62]. In this case, the particle-hole symmetry appears naturally as it is a consequence of the up-down symmetry of the spin Hamiltonian in the absence of an external magnetic field. Such a magnetic realization of a Mott glass (albeit in three dimensions) was recently observed in bromine-doped dichloro-tetrakis-thiourea-nickel (DTN)[9].

[1] B. C. Crooker, B. Hebral, E. N. Smith, Y. Takano, and J. D. Reppy, Phys. Rev. Lett. **51**, 666 (1983).

[2] J. D. Reppy, Physica B+C **126**, 335 (1984).

[3] H. S. J. van der Zant, F. C. Fritschy, W. J. Elion, L. J. Geerligs, and J. E. Mooij, Phys. Rev. Lett. **69**, 2971 (1992).

[4] H. S. J. van der Zant, W. J. Elion, L. J. Geerligs, and J. E. Mooij, Phys. Rev. B **54**, 10081 (1996).

[5] D. B. Haviland, Y. Liu, and A. M. Goldman, Phys. Rev. Lett. **62**, 2180 (1989).

[6] A. F. Hebard and M. A. Paalanen, Phys. Rev. Lett. **65**, 927 (1990).

[7] A. Oosawa and H. Tanaka, Phys. Rev. B **65**, 184437 (2002).

[8] T. Hong, A. Zheludev, H. Manaka, and L.-P. Regnault, Phys. Rev. B **81**, 060410 (2010).

[9] R. Yu, L. Yin, N. S. Sullivan, J. S. Xia, C. Huan, A. Paduan-Filho, N. F. O. Jr, S. Haas, A. Steppke, C. F. Miclea, F. Weickert, R. Movshovich, E.-D. Mun, B. L. Scott, V. S. Zapf, and T. Roscilde, Nature **489**, 379 (2012).

[10] M. White, M. Pasienski, D. McKay, S. Q. Zhou, D. Ceperley, and B. DeMarco, Phys. Rev. Lett. **102**, 055301 (2009).

[11] S. Krinner, D. Stadler, J. Meineke, J.-P. Brantut, and T. Esslinger, Phys. Rev. Lett. **110**, 100601 (2013).

[12] C. D'Errico, E. Lucioni, L. Tanzi, L. Gori, G. Roux, I. P. McCulloch, T. Giamarchi, M. Inguscio, and G. Modugno, Phys. Rev. Lett. **113**, 095301 (2014).

[13] D. S. Fisher and M. P. A. Fisher, Phys. Rev. Lett. **61**, 1847 (1988).

[14] M. P. A. Fisher, P. B. Weichman, G. Grinstein, and D. S. Fisher, Phys. Rev. B **40**, 546 (1989).

[15] L. Pollet, N. V. Prokof'ev, B. V. Svistunov, and M. Troyer, Phys. Rev. Lett. **103**, 140402 (2009).

[16] R. B. Griffiths, Phys. Rev. Lett. **23**, 17 (1969).

[17] M. Thill and D. A. Huse, Physica A **214**, 321 (1995).

[18] T. Vojta, J. Phys. A **39**, R143 (2006).

[19] P. B. Weichman and R. Mukhopadhyay, Phys. Rev. Lett. **98**, 245701 (2007).

[20] A. Priyadarshee, S. Chandrasekharan, J.-W. Lee, and H. U. Baranger, Phys. Rev. Lett. **97**, 115703 (2006).

[21] H. Meier and M. Wallin, Phys. Rev. Lett. **108**, 055701 (2012).

[22] R. Ng and E. S. Sørensen, Phys. Rev. Lett. **114**, 255701 (2015).

[23] J. P. Álvarez Zúñiga, D. J. Luitz, G. Lemarié, and N. Laflorencie, Phys. Rev. Lett. **114**, 155301 (2015).

[24] T. Giamarchi, P. Le Doussal, and E. Orignac, Phys. Rev. B **64**, 245119 (2001).

[25] P. B. Weichman and R. Mukhopadhyay, Phys. Rev. B **77**, 214516 (2008).

[26] N. Prokof'ev and B. Svistunov, Phys. Rev. Lett. **92**, 015703 (2004).

[27] Here, the numbers in parentheses are the errors of the last digits.

[28] S. Iyer, D. Pekker, and G. Refael, Phys. Rev. B **85**, 094202 (2012).

[29] M. Swanson, Y. L. Loh, M. Randeria, and N. Trivedi, Phys. Rev. X **4**, 021007 (2014).

[30] M. Guo, R. N. Bhatt, and D. A. Huse, Phys. Rev. Lett. **72**, 4137 (1994).

[31] H. Rieger and A. P. Young, Phys. Rev. Lett. **72**, 4141 (1994).

[32] R. Sknepnek, T. Vojta, and M. Vojta, Phys. Rev. Lett. **93**, 097201 (2004); T. Vojta and R. Sknepnek, Phys. Rev. B. **74**, 094415 (2006).

[33] T. Vojta and J. Schmalian, Phys. Rev. Lett. **95**, 237206 (2005).

[34] M. Wallin, E. S. Sorensen, S. M. Girvin, and A. P. Young, Phys. Rev. B **49**, 12115 (1994).

[35] M. Campostrini, M. Hasenbusch, A. Pelissetto, and E. Vicari, Phys. Rev. B **74**, 144506 (2006).

[36] A. B. Harris, J. Phys. C **7**, 1671 (1974).

[37] M. N. Barber, in *Phase Transitions and Critical Phenomena*, Vol. 8, edited by C. Domb and J. L. Lebowitz (Academic, New York, 1983) pp. 145–266.

[38] J. Cardy, ed., *Finite-size scaling* (North Holland, Amsterdam, 1988).

[39] D. S. Fisher, Phys. Rev. Lett. **69**, 534 (1992); Phys. Rev. B **51**, 6411 (1995).

[40] J. A. Hoyos, C. Kotabage, and T. Vojta, Phys. Rev. Lett. **99**, 230601 (2007); T. Vojta, C. Kotabage, and J. A. Hoyos, Phys. Rev. B **79**, 024401 (2009).

[41] A. Del Maestro, B. Rosenow, M. Müller, and S. Sachdev, Phys. Rev. Lett. **101**, 035701 (2008); A. Del Maestro, B. Rosenow, J. A. Hoyos, and T. Vojta, **105**, 145702 (2010).

[42] Y. Xing, H.-M. Zhang, H.-L. Fu, H. Liu, Y. Sun, J.-P. Peng, F. Wang, X. Lin, X.-C. Ma, Q.-K. Xue, J. Wang, and X. C. Xie, Science **350**, 542 (2015).

[43] S. Ubaid-Kassis, T. Vojta, and A. Schroeder, Phys. Rev. Lett. **104**, 066402 (2010).

[44] T. Vojta, J. Low Temp. Phys. **161**, 299 (2010).

[45] T. Vojta and J. Schmalian, Phys. Rev. B **72**, 045438 (2005).

[46] F. Cooper, B. Freedman, and D. Preston, Nucl. Phys. B **210**, 210 (1982).

[47] J. K. Kim, Phys. Rev. Lett. **70**, 1735 (1993).

[48] S. Caracciolo, A. Gambassi, M. Gubinelli, and A. Pelissetto, Eur. Phys. J. B **20**, 255 (2001).

[49] U. Wolff, Phys. Rev. Lett. **62**, 361 (1989).

[50] N. Metropolis, A. Rosenbluth, M. Rosenbluth, and A. Teller, J. Chem. Phys. **21**, 1087 (1953).

[51] H. G. Ballesteros, L. A. Fernández, V. Martín-Mayor, A. Muñoz Sudupe, G. Parisi, and J. J. Ruiz-Lorenzo, Phys. Rev. B **58**, 2740 (1998).

[52] H. G. Ballesteros, L. A. Fernandez, V. Martin-Mayor, A. Munoz Sudupe, G. Parisi, and J. J. Ruiz-Lorenzo, Nucl. Phys. B **512**, 681 (1998).

[53] Q. Zhu, X. Wan, R. Narayanan, J. A. Hoyos, and T. Vojta, Phys. Rev. B **91**, 224201 (2015).

[54] T. Vojta and J. A. Hoyos, in *Recent Progress in Many-Body Theories*, edited by J. Boronat, G. Astrakharchik, and F. Mazzanti (World Scientific, Singapore, 2008) p. 235.

[55] For low dilutions p, the parabola fits of g_{av} vs. L_τ are affected by corrections to scaling for small L and L_τ. We thus slightly adjust L_τ^{max} and g_{av}^{max} to further improve the quality of the data collapse onto a common master curve. This applies to the four smallest system sizes L for $p = 1/8$ and $1/5$ and the three smallest sizes for $p = 2/7$. The resulting change of the value of z is about 0.01, well below the error due to the uncertainty in T_c.

[56] J. T. Chayes, L. Chayes, D. S. Fisher, and T. Spencer, Phys. Rev. Lett. **57**, 2999 (1986).

[57] N. Prokof'ev and B. Svistunov, Phys. Rev. Lett. **87**, 160601 (2001).

[58] We actually use $z = 1.45$ which is close to the effective dynamical exponent found for the system size range and dilution considered.

[59] O. Motrunich, S. C. Mau, D. A. Huse, and D. S. Fisher, Phys. Rev. B **61**, 1160 (2000).

[60] E. Altman, Y. Kafri, A. Polkovnikov, and G. Refael, Phys. Rev. B **81**, 174528 (2010).

[61] Y. Wang, W. Guo, and A. W. Sandvik, Phys. Rev. Lett. **114**, 105303 (2015).

[62] T. Roscilde and S. Haas, Phys. Rev. Lett. **99**, 047205 (2007).